

# High-latitude eddy covariance temporal network design and optimization.

Martijn Pallandt<sup>1</sup>, Martin Jung<sup>2</sup>, Kyle A Arndt<sup>3</sup>, Susan M. Natali<sup>3</sup>, Brendan Rogers<sup>3</sup>, Anna- Maria Virkkala<sup>4</sup>, and Mathias Göckede<sup>5</sup>

<sup>1</sup>Max Planck Institute for Biogeochemistry

<sup>2</sup>Max-Planck-Institute for Biogeochemistry

<sup>3</sup>Woodwell Climate Research Center

<sup>4</sup>Woodwell Climate Research Center, Falmouth, MA, USA

<sup>5</sup>Max-Planck Institute for Biogeochemistry

October 17, 2023

## Abstract

Ecosystems at high latitudes are under increasing stress from climate change. To understand changes in carbon fluxes, in situ measurements from eddy covariance networks are needed. However, there are large spatiotemporal gaps in the high-latitude eddy covariance network. Here we used the relative extrapolation error index in machine learning-based upscaled gross primary production as a measure of network representativeness and as the basis for a network optimization. We show that the relative extrapolation error index has steadily decreased from 2001 to 2020, suggesting diminishing upscaling errors. In experiments where we limit site activity by either setting a maximum duration or by ending measurements at a fixed time those errors increase significantly, in some cases setting the network status back more than a decade. Our experiments also show that with equal site activity across different theoretical network setups, a more spread out design with shorter-term measurements functions better in terms of larger-scale representativeness than a network with fewer long-term towers. We developed a method to select optimized site additions for a network extension, which blends an objective modeling approach with expert knowledge. Using a case study in the Canadian Arctic we show several optimization scenarios and compare these to a random site selection among reasonable choices. This method greatly outperforms an unguided network extension and can compensate for suboptimal human choices. Overall, it is important to keep sites active and where possible make the extra investment to survey new strategic locations.

## Hosted file

975437\_0\_art\_file\_11438407\_s1r2sd.docx available at <https://authorea.com/users/670634/articles/670512-high-latitude-eddy-covariance-temporal-network-design-and-optimization>

## Hosted file

975437\_0\_supp\_11438408\_s1r2sd.docx available at <https://authorea.com/users/670634/articles/670512-high-latitude-eddy-covariance-temporal-network-design-and-optimization>

## High-latitude eddy covariance temporal network design and optimization.

Martijn M.T.A. Pallandt<sup>1</sup>, Martin Jung<sup>2</sup>, Kyle Arndt<sup>3</sup>, Susan Natali<sup>3</sup>, Brendan M. Rogers<sup>3</sup>, Anna-Maria Virkkala<sup>3</sup>, Mathias Göckede<sup>1</sup>

<sup>1</sup>Department of Biogeochemical Signals, Max Planck Institute for Biogeochemistry, Jena, 07745, GER

<sup>2</sup>Department of Biogeochemical Integration, Max Planck Institute for Biogeochemistry, Jena, 07745, GER

<sup>3</sup>Woodwell Climate Research Center, Falmouth, MA 02540, USA

Corresponding author: Martijn Pallandt ([mpall@bgc-jena.mpg.de](mailto:mpall@bgc-jena.mpg.de))

### Key Points:

- The network of high-latitude eddy covariance sites has grown considerably over time, still towers should remain active and new remote locations added.
- Without new measurements our knowledge will degrade at a rate at least equal to which would otherwise be its growth.
- Network optimization methods as shown here are essential for representative network design.

### Abstract

Ecosystems at high latitudes are under increasing stress from climate change. To understand changes in carbon fluxes, in situ measurements from eddy covariance networks are needed. However, there are large spatiotemporal gaps in the high-latitude eddy covariance network. Here we used the relative extrapolation error index in machine learning-based upscaled gross primary production as a measure of network representativeness and as the basis for a network optimization. We show that the relative extrapolation error index has steadily decreased from 2001 to 2020, suggesting diminishing upscaling errors. In experiments where we limit site activity by either setting a maximum duration or by ending measurements at a fixed time those errors increase significantly, in some cases setting the network status back more than a decade. Our experiments also show that with equal site activity across different theoretical network setups, a more spread out design with shorter-term measurements functions better in terms of larger-scale representativeness than a network with fewer long-term towers. We developed a method to select optimized site additions for a network extension, which blends an objective modeling approach with expert knowledge. Using a case study in the Canadian Arctic we show several optimization scenarios and compare these to a random site selection among reasonable choices. This method greatly outperforms an unguided network extension and can compensate for suboptimal human choices. Overall, it is important to keep sites active and where possible make the extra investment to survey new strategic locations.

## 39 **1 Introduction**

40 The Arctic and boreal biomes have been recognized as a domain that is changing rapidly  
41 as a result of climate change (Serreze & Barry, 2011; IPCC, 2014; Meredith et al., 2019). These  
42 changes may lead to strong positive feedbacks with ongoing climate change, since large stocks  
43 of carbon sequestered in soils may become unstable as permafrost thaws (Gustaf Hugelius et al.,  
44 2020; E. A. G. Schuur et al., 2015; Edward A. G. Schuur et al., 2008; Serreze & Barry, 2011).  
45 For reliable forecasts of future global climate, it is of vital importance to monitor the carbon  
46 cycle in these regions and understand the mechanisms that govern it.

47

48 Eddy covariance (EC) is a key technique to investigate the carbon cycle. With this  
49 method, fluxes of greenhouse gasses (GHG), predominantly carbon dioxide (CO<sub>2</sub>) and methane  
50 (CH<sub>4</sub>, and energy are measured continuously at high temporal resolution above the canopy to  
51 quantify their rate of exchange between the atmosphere and biosphere (Baldocchi, 2003;  
52 Pastorello et al., 2020; Sulkava et al., 2011). The typical field of view, or footprint area, for EC  
53 towers found in most parts of the Arctic is relatively small, usually on the scale of hundreds of  
54 meters, (Göckede et al., 2004; Kljun et al., 2002; Rannik et al., 2000; Schmid, 1997; Vesala et  
55 al., 2008). To obtain regional carbon budgets, these local measurements need to be upscaled to  
56 much larger domains. There are varied methods to upscale fluxes, which have greatly improved  
57 over the years (Byrne et al., 2023; Chu et al., 2021; Desai, 2010; Jung et al., 2011; Xiao et al.,  
58 2012) with some specifically targeting the Arctic (Birch et al., 2021; Ito et al., 2023; Peltola et  
59 al., 2019; Virkkala et al., 2021). Of these methods, machine learning techniques are becoming  
60 increasingly important. Still, no matter how advanced the methods, the fluxes used either as  
61 input or reference should cover the relevant range of conditions and ecosystem types; otherwise  
62 prediction accuracy can neither be guaranteed nor properly assessed. Therefore, location and  
63 coverage of the EC towers should be carefully considered in any upscaling endeavor.

64

65 Typically, EC towers have been placed to answer specific research questions, while the  
66 role of a given tower in the larger observational network plays a minor role in decision making  
67 and funding. Moreover, site selection is often strongly constrained by logistical considerations  
68 and available infrastructure. This has led to a site distribution in the Arctic that greatly favors  
69 Alaska and Europe, often at locations with access to electricity, leaving large areas of northern  
70 Canada and Siberia undersampled (Pallandt et al., 2022). When evaluating tower infrastructure  
71 for wintertime CO<sub>2</sub> fluxes, or CH<sub>4</sub> fluxes, we see even larger gaps across these regions, with  
72 wintertime representativeness values 74% worse and CH<sub>4</sub> 48% worse than the summertime CO<sub>2</sub>  
73 measurements (Pallandt et al., 2022). The establishment of a long time series of flux  
74 measurements is another major challenge: Typically, funding for EC towers is provided on a  
75 project basis, which typically guarantees funding only for a couple of years. Researchers cobble  
76 together grants to keep towers active for longer, though this is not an ideal basis for a stable  
77 monitoring network. Research Infrastructures like ICOS and NEON aim to alleviate this problem  
78 by advocating for long-term data collection and flux data standardization, however these are only  
79 active in Europe and the USA respectively, and even there not all EC towers fall under their  
80 umbrella. Overall, the future of most EC sites is highly uncertain.

81

82 Several studies have investigated the representativeness of EC networks, and in some  
83 cases, virtually extended these networks by including mechanics to optimize the spatial  
84 distribution of the network in case of potential future extension (Chu et al., 2021; Hoffman et al.,  
85 2013; Pallandt et al., 2022; Sulkava et al., 2011; Villarreal & Vargas, 2021). Still, no studies  
86 have investigated the representativeness of the EC network in relation to long-term temporal data  
87 coverage. Pallandt et al. (2022) looked at the differences between the winter- and summertime  
88 network representativeness, though only in terms of differences in the spatial component. Still  
89 temporal changes are important for the EC network. The longer a monitoring network remains  
90 active and expands, the more data it will accumulate, which in turn increases its capabilities to  
91 interpolate within its dataspace or extrapolate beyond it (Banko & Brill, 2001; Bosveld &  
92 Beljaars, 2001; Loescher et al., 2006; Wisz et al., 2008), though as climate changes, we are  
93 entering non-analog climate conditions which past towers may not fully represent. It remains to  
94 be quantified how the growing coverage period of an existing network, associated with more  
95 accumulated data over time for the same subset of sites, changes our ability to upscale fluxes.  
96 This information is crucial to guide us in maintaining and upgrading the network with increased  
97 efficiency.

98

99 In this paper, we aim to quantify the EC network representativeness potential for  
100 upscaling flux data to a larger domain, in relation to temporal factors. As a starting point for our  
101 analysis, we update the existing high-latitude EC meta-database used in Pallandt et al. (2022)  
102 through further evaluation of meta-data and an updated survey. We then extend the extrapolation  
103 index metric first shown in Jung et al. (2020) by including an optimization scheme to investigate  
104 network growth and expansion. We use these methods to investigate how choices in the temporal  
105 arrangement of the network can affect its representativeness. We do this through several  
106 experiments that each test a specific temporal aspect of the network's design and functioning:  
107 termination of measurements, limitation of site activity to a few seasons and the tradeoff between  
108 few long term and many shorter measurements. Finally we demonstrate a practical application of  
109 these techniques in a case study where we combine modeled optimization with expert knowledge  
110 in an actual potential network extension.

## 111 **2 Methods**

### 112 2.1 Network status

113 To update our database on high-latitude EC towers to reflect the current status up to  
114 2022, we updated the survey conducted by Pallandt et al. (2022) in 2017 and added more specific  
115 questions about a given site's biome, planned future activity and future funding as well as  
116 extending the site activity table to 2022. The survey was distributed among the FLUXNET  
117 newsletter members and known PIs of high-latitude EC sites. Counting direct correspondence to  
118 the survey as well as submissions to the online form we received 37 replies. Combined with our  
119 previous results, we now have temporally explicit information for 88 sites from 1993 when the  
120 first towers in the Arctic were erected, though not all cover the period from 2018 to 2022.  
121 Combining these further with online sources such as the flux databases (e.g., AmeriFlux,  
122 AsiaFlux, Fluxnet, ICOS, NEON), personal communication, and collaborating database projects  
123 (ABCflux, Virkkala et al. (2022)) we added or updated information on a total of 145 EC sites in  
124 comparison to the previous database version. This database is available at the high-latitude

125 carbon flux tool: <https://cosima.nceas.ucsb.edu/carbon-flux-sites/>, which, besides metadata on  
126 EC flux sites, also lists metadata on flux chambers and atmospheric towers.

127

128 While Pallandt et al. (2022) limited the study domain to areas above 60 degrees North, in  
129 this study we opted for a more natural southern border that follows the extent of Tundra and  
130 Boreal biomes (58 ecoregions) as defined by Dinerstein et al. (2017), which is an update of  
131 (Olson et al., 2001); details on the domains can be found in figure S2 and table S2.1. By setting  
132 the cutoff of the domain based on bioclimatic conditions, we reduce the risk of excluding sites –  
133 especially near domain borders – that would be relevant to our representativeness assessment.  
134 And through the inclusion of these ecoregions, we can more specifically target and describe  
135 regions of interest throughout this work.

## 136 2.2 Extrapolation error

137 The extrapolation error index (EI) metric aims to quantify the relative increase in  
138 upscaled flux error as a function of increased distance (in predictor variable space) to the nearest  
139 flux measurements used for training, it is conceptually very similar to the Dissimilarity Index  
140 from Meyer & Pebesma (2021). For details on the EI method please refer to supplement S2 of  
141 Jung et al. (2020), while a short summary follows here for the reader's convenience.

142

143 The procedure of estimating EI consists of two steps: 1) Estimating the distance in  
144 predictor space between a predicted data point to the nearest training data points, and 2)  
145 estimating how the prediction error increases with distance from training data to yield a  
146 normalization of this distance. In the first step, weights for predictors variables (to account for  
147 different variable importances) and the considered number of nearest training data points is  
148 established by an optimization algorithm.

149 The predictor data space is a set of variables representing the conditions observed at the  
150 EC sites, which, in our case, are the nine predictors in the FLUXCOM-RS upscaling model  
151 ensemble (Jung et al. 2020, Tramontana et al. 2016, Table 1). The target variable is GPP from  
152 FLUXCOM-RS extracted at the locations of available EC sites. The entireThis process of  
153 training the model and calculating EI values is repeated 7 times in an ensemble to make the  
154 results more robust. Three separate training runs have beenbene performed: one for the temporal  
155 experiments, one for optimization runs and one for the comparison with previous work (S5).

156

157 **Table 1: variables used in the calculation of the EI. All variables are provided in a global**  
158 **grid at 0.0833 degrees spatial resolution. Unless otherwise stated, the temporal range is**  
159 **from 2001 to 2020 with monthly steps, others are either static or a climatology of 12**  
160 **months. All predictor variables are available at the Max Planck Institute for**  
161 **Biogeochemistry Data Portal file id 260. For a description of the quality flags and gap**  
162 **filling approaches used see (Jung et al., 2020)**  
163

Variable	Original Source/ MODIS ID	Temporal resolution
----------	---------------------------	---------------------

Nadir Reflectance Band7	MCD43B4.006.v4_201905	static
Enhanced Vegetation Index	MOD13A2	static
Day Time Land Surface Temperature	MOD11A2	monthly
Night Time Land Surface Temperature	MOD11A2	monthly
Maximum Day Time Land Surface Temperature	MOD11A2	static
Land Cover Data +C4 fraction croplands	MCD12Q1	static
Fraction of photosynthetically active radiation	MOD15A2	climatology
Normalized Difference Vegetation Index * Rg	MOD13A2	monthly
NDWI Normalized difference water index	MCD43A4	monthly
Gross Primary Productivity - RS	Jung et al. (2020)	monthly

### 164 2.3 Temporal effects

165 We performed several experiments to assess the effect of variations in site activity on the  
166 network's EI (see table S3 for an overview). For means of comparison, we first established a base  
167 scenario (**Baseline**), which formed the network setup against which all other runs were  
168 compared. It represents the full EC network as it has grown from 2001 to 2020, with extra data  
169 added to those available previously, just as the dataset of measurements increases over time. Site  
170 activity was assigned in several steps: years of sites for which we have explicit monthly activity  
171 status required no further steps, while years of sites with known wintertime activity were  
172 assumed to be active throughout all the months within the year. For the remaining sites years, we  
173 assumed “summertime-only” activity, with data coverage restricted to the months. The following  
174 setups differ from Baseline only in aspects listed below.

175

176 As a first scenario, to gauge how the network would be affected in the hypothetical  
177 absence of new measurements, we performed the **End10** and **End15** runs. These runs progressed  
178 exactly as the baseline case, except all measurements were terminated at the start of 2010 and  
179 2015, respectively. From these points onwards the extrapolation could only utilize past data. This  
180 experiment not only reflects potential gaps in data acquisition or even termination of sites but  
181 could also serve as a measure of the trajectory of uncertainties as temporal distance to the last  
182 measurement increases when extrapolating into the future.

183

184 In the second scenario, we assessed the effect of limiting site activity to quantify how  
185 much the EI increases if sites would only be active for a limited duration, e.g., in the framework  
186 of a typical research project. These runs are called **MaxX** where X reflects the maximum number  
187 of months sites were allowed to remain active. In these scenarios, for each site we tracked their  
188 activity and quit any sampling after the allotted number of active months was completed. Here  
189 the **Max12** run represents a full year of measurements, while **Max18** corresponds to three years

190 of summertime measurements. Finally, **Max36** represents three full years of measurements. The  
191 three year mark was chosen in correspondence with the survey which indicated this project  
192 duration as a period for which most sites had funding.

193

194 As a third scenario, we investigated the relative impact of site month distribution over the  
195 network, where one site month represents one site being active for one month. For this purpose,  
196 we compared the performance of a network with fewer sites with long activity (depth) to that of  
197 a network with many sites with shorter activity (breadth). In both cases, the amount of data  
198 supplied for the analysis ( i.e. the total number of site months considered) was uniform. These  
199 depth versus breadth runs **DvB10**, **DvB15** and **DvB20** were based on the networks' total site  
200 months in 2010, 2015 and 2020, respectively. The number of sites ranges from 55 (largest depth)  
201 to 127 (largest breadth), modifying site number in steps of 12 in between. To keep site months  
202 consistent among each of the setups, we had to adjust actual site activity. For example, in the  
203 case of a network with 55 sites, all of these sites would typically be active all the time year  
204 round. In order to keep a realistic distribution of site activity under these conditions, we  
205 developed a pseudorandom data month distribution among the existing site locations as  
206 explained in supplement 1.

## 207 2.4 Network optimization

208 To allow the use of our network evaluation tool for the purpose of strategic observation  
209 network expansion, we added routines that allow for the optimized addition of sites to an existing  
210 network. We test 3 methods here, in all cases starting with the baseline of the current network. In  
211 order not to confuse this with the 20-year baseline runs from the temporal effects section, we  
212 name this baseline EI\_ref. It represents the EI calculated for the network in its 2022 state based  
213 on the monthly climatology used in comparison to previous work. Three optimization methods  
214 were tested, we eventually used a greedy optimization method which evaluates the EI for all  
215 potential candidate sites individually. The algorithm then selects the one site which generates the  
216 lowest mean EI over the domain and adds it to the existing network. After updating the baseline  
217 for the extended network, the same steps are repeated sequentially, adding one site at a time until  
218 none are left in the list of candidate sites. This method is fast, but the independent step-by-step  
219 additions cannot guarantee that the optimal site combination is chosen for more than 1 additional  
220 site; however, the other two methods (S4) are too computationally expensive to optimize for  
221 more than 7 site additions, and this greedy method resulted in the same site selection where we  
222 were able to compare.

223

224 This method only considers a site's EI impact, though often there are many more  
225 considerations that play a role in site selection such as logistic feasibility, a site's history, other  
226 research demands etc. Many of these requirements are hard to quantify, and even if quantified,  
227 weighing them would be fairly objective making a numerical approach undesirable for these  
228 extra considerations. This where an expert would come in such as the PI, they could for example  
229 decide between similar sites in regard to network improvement which additional requirements  
230 would be a deciding factor in choosing a new location. To facilitate this process, we added  
231 further metrics that aid the expert to make informed decisions, where if less than ideal sites are  
232 chosen site similarity and loss of improvement can be considered. We compute the similarity

233 between sites as the Euclidean distance between all sites based on the local summertime  
234 predictor values. To make the distance metric more intuitive, clusters are created based on these  
235 distances following the wards method of hierarchical clustering (Ward, 1963), in which we  
236 choose a cutoff that results in 5 clusters that roughly represent a north-south gradient. This  
237 information is then combined with the EI metric to show optimal sites and all subsequent less  
238 than ideal sites in plots such as figure 5 to create a comprehensive view of all options. In  
239 subsequent model runs the preselected sites can be added which the model will then take into  
240 account.  
241

## 242 2.5 Regional case study for network optimization

243 In a case study, we used optimization methods described above to guide the improvement  
244 of the high-latitude EC network within Canada. As an additional goal, this extension was aiming  
245 at the establishment of a north-to-south transect of EC sites that would characterize the transition  
246 of forests in warmer climates to the wetlands and treeless tundra in the colder climates. As a first  
247 step, a selection of potential sites was made based on proximity to populated places within the  
248 target region, and sites in our database that were no longer active. This resulted in a list of 28  
249 potential new sites (listed in Fig. 6 and table S2.2). The EI\_ref run showed the EI of the domain  
250 based on the network's EC site activity in 2022, which is used as the basis for further  
251 optimizations. Several optimization runs were then performed to gain a better idea of the impact  
252 of site selection:

- 253 • Free search: This approach considered all potential sites in Canada.
- 254 • Fixed search: Using the same subset as the free search, the Iqaluit, Churchill Fen  
255 and Reservoir site were selected before starting a 'free' optimization. Iqaluit was  
256 included at the start because it had the highest positive impact on the EI and it is  
257 logistically optimally located. The latter two sites were selected here because their  
258 inclusion had been predetermined for other reasons unrelated to network  
259 optimization.
- 260 • Free exclude search: this approach was similar to 'free search' run, except seven  
261 sites were excluded prior to network optimization. The Mackenzie river region is  
262 fairly well represented thus we focus on Eastern Canada in this case. And we  
263 removed sites that after further investigation currently lacked the right  
264 infrastructure for EC towers.

265

266 As a benchmark of the optimization, we evaluated a random allocation instead of an  
267 optimized one. For each number of site additions ( $n = [1, 28]$ ), 1000 random site combinations  
268 are tested. The highest, mean and lowest domain wide EI means of these randomized trials were  
269 calculated. In cases where there were less than 1000 combinations possible ( $2 \geq n \geq 26$ ), we  
270 evaluated all combinations.

271 **3 Results**

## 272 3.1 Network status

273 The network of high-latitude EC sites has grown significantly over the past 29 years  
274 (1993 to 2022) to a total of 213 EC sites being active at least periodically within the boreal and  
275 Arctic domain. Of these sites, 119 were active in 2022, and 44 of these remain active throughout  
276 the winter months (Figure 1). Sixty-six out of 213 sites feature methane measurements, but only  
277 45 of these sites are active. By the end of 2022 the network has accumulated a total of 15048 site  
278 months (Figure 1) assuming unspecified monthly or wintertime activity means they are only  
279 active during the summer months. Regarding funding and planned future activity, of the 22  
280 respondents that answered this question in our latest survey, 59% indicated they plan to remain  
281 active for 5 years or more, and when only considering sites that are currently active this  
282 increased to 76%. When asked how long their funding lasts, PIs that planned to keep their sites  
283 active for 5 years or more had funding secured for a mean of 3.1 years.

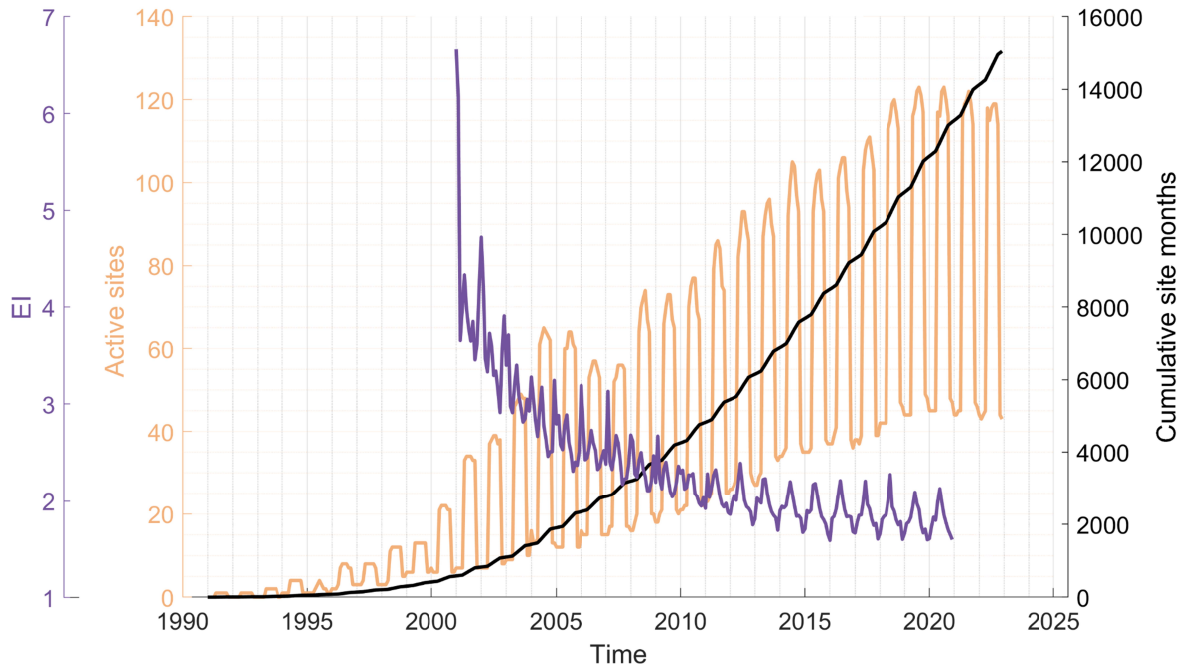
284

285 We evaluated the growth of the network in detail from 2001 to 2020. In this period, the  
286 summer activity increased from 34 sites in 2001 to 123 in 2020, while winter site activity  
287 underwent a larger relative change from 7 sites to 44 on average. Over these 20 years, on average  
288 sites were kept active for 63 months (~5.3 years), with 17 sites active throughout the entire 20-  
289 year period though these sites typically have wintertime shutdowns.

290

291 For each of the 240 months from 2001 to 2020, we calculated the EI based on the  
292 cumulative collected data up until that point. The yearly mean EI dropped from 3.0 to 1.2 (Figure  
293 S4.a, Video S6), indicating the mean extrapolation error more than halved during this period.  
294 Domain wide pixel based minimum values decreased substantially from 0.12 to 0.0. Maximum  
295 values have mostly stayed at a high level, dropping from 20.3 to 15.7 in the first four years and  
296 then to 14.7 in the subsequent 16 years. This indicates that while the extension of the network  
297 and the longer time series improved our capability for upscaling in most regions, only minor  
298 improvements were obtained in some of the most remote or extreme locations.

299



300  
 301 **Figure 1. Network growth over time. EI in purple on the leftmost axis shows the mean**  
 302 **domain wide extrapolation index per month from 2001 to 2020 which is the timeframe for**  
 303 **which FLUXCOM predictor data is available. Active sites in yellow on the left axis graph**  
 304 **the site activity per month, a clear annual pattern is visible between winter and summer**  
 305 **site activity. Cumulative site months are shown in black, with scale on the right axis in the**  
 306 **same color.**

307

308 The EI, and changes therein over time, are not uniform throughout the domain. In the  
 309 final year of our assessment, the worst and best represented ecoregion, respectively, are both  
 310 located in Canada: the *Muskwa-Slave Lake taiga* ecoregion had an average EI of 0.92, whereas  
 311 the *Canadian High Arctic tundra* had the highest EI rating at 1.99. The greatest improvement  
 312 over 20 years was observed in the Russian Arctic desert, where EI was reduced by 3.27, i.e.,  
 313 from 5.04 to 1.77. Over the same period, in the *Midwest Canadian Shield forests* an  
 314 improvement of only 0.60 is detected.

315

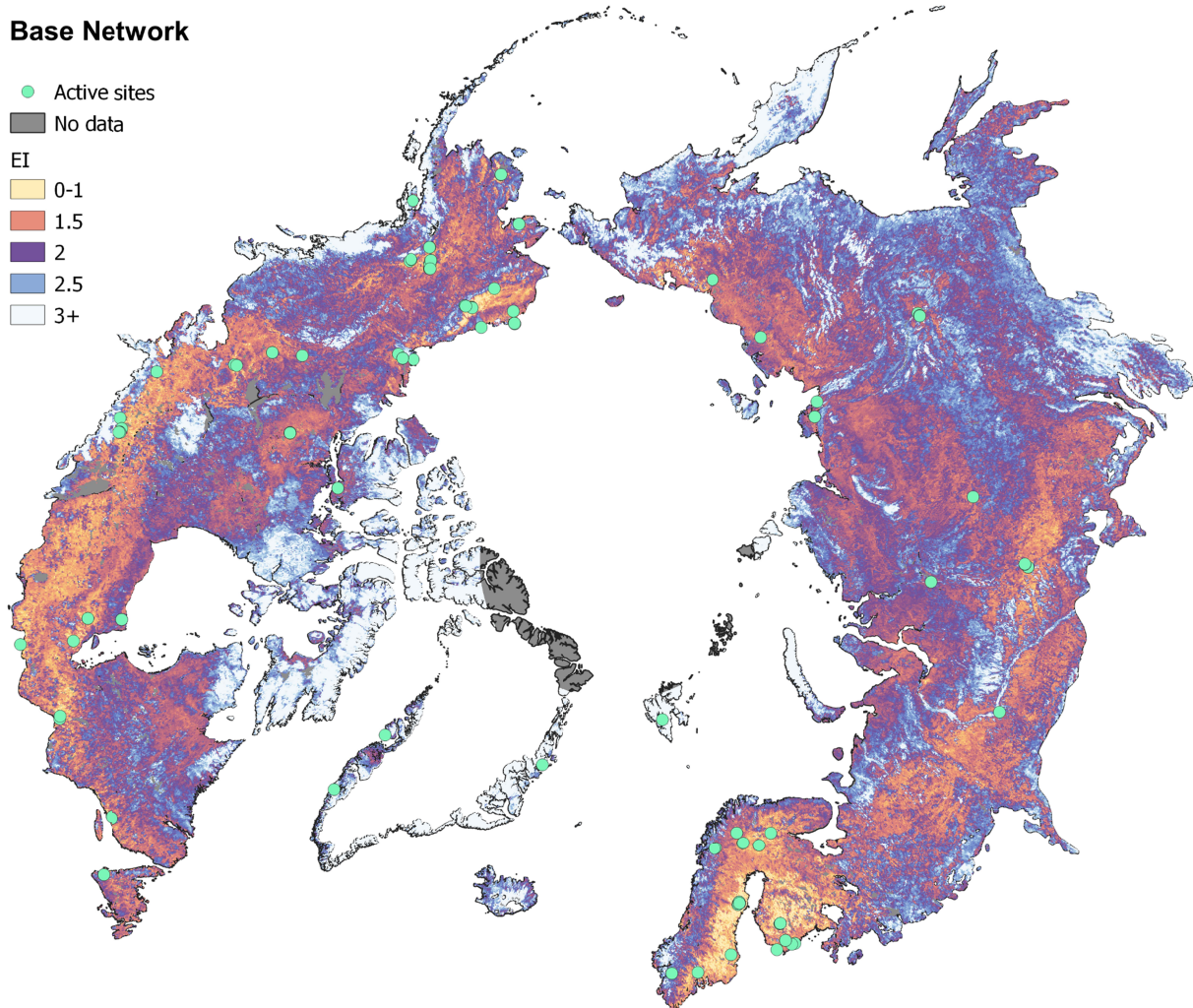
316 Of note is that there is a difference in summer- and wintertime EI. From 2001 until 2004,  
 317 summertime EI was lower than wintertime EI, from 2004 until 2011 we calculated similar values  
 318 for both, whereas from 2011 and onward the situation reversed, and wintertime EI values were  
 319 lower than summertime EI. Overall, the expansion of the network has resulted in an improved  
 320 representativeness in all regions and for all seasons. And even though with an ever-growing  
 321 network improving it becomes more challenging to find new high-impact locations, there is still  
 322 room for expansion, particularly if new sites are being placed strategically. In response to these  
 323 observed differences, we investigated differences in spatial and temporal variation between  
 324 Winter and Summer (table 2). Two of the four temporally explicit variables, NDVIRg and  
 325 NDWI, as well as GPP, show considerably lower means and standard deviations for winter  
 326 conditions as compared to summer. Meaning that in wintertime the domain is more spatially

327 homogeneous, and thus with lower variation in the predictors less observation points are  
 328 required.  
 329

330 **Table 1. Median and standard deviations of yearly and monthly explicit predictor variables**  
 331 **data over the entire domain. Summer is defined as April through September whereas the**  
 332 **remaining months are assigned as Winter. The Overall columns list statistics for all data.**  
 333 **The Spatial columns list the mean standard deviation for each time step over the entire**  
 334 **domain. The Temporal columns list the mean standard deviation for each location over all**  
 335 **time steps. GPP, NDVIRg and NDWI, clearly show in all cases smaller mean and std in**  
 336 **winter compared to summer.**  
 337

Variable	Overall				Spatial		Temporal	
	Winter mean	Summer mean	Winter std	Summer std	Winter std	Summer std	Winter std	Summer std
Gross Primary Productivity	0.07	2.26	0.14	2.15	0.09	1.48	0.08	1.50
Day Time Land Surface Temperature	253	283	11.1	11.4	8.26	6.80	8.22	9.57
Night Time Land Surface Temperature	250	274	10.2	9.46	7.79	5.05	7.41	8.26
Normalized Difference Vegetation Index * Rg	0.30	6.44	0.78	5.22	0.57	3.69	0.46	3.92
NDWI Normalized difference water index	0.23	0.08	0.10	0.19	0.08	0.13	0.08	0.17

338

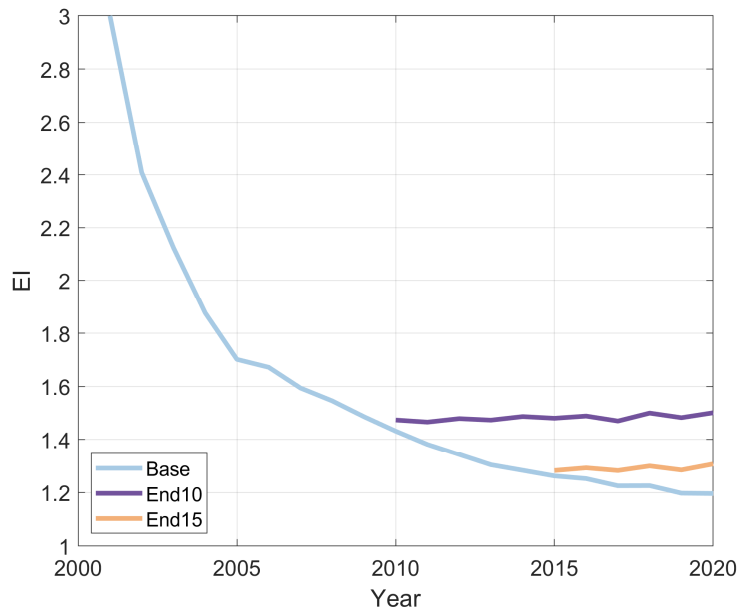


339  
 340 **Figure 2. EI of the network in its 2022 state based on one year climatology. Yellow indicates**  
 341 **a low EI thus low errors indicating better representativeness whereas colder colors (blue to**  
 342 **white) indicate underrepresented areas with high EI ratings. Green dots show the locations**  
 343 **of EC sites and grayed out areas indicate no data regions from 80 degrees North and up.**

### 344 3.2 Temporal effects

345 In the End10 and End15 scenarios, we investigated how a hypothetical termination of  
 346 measurements (after in 2010 and 2015 respectively) would affect our capability of upscaling  
 347 fluxes in the domain (Figure S4 b-c). Compared to the baseline scenario, in the End10 scenario  
 348 the EI increased on average by 0.005 per year ( $p > 0.01$   $n=11$ ) for a total increase of EI by 0.08  
 349 in 2020. For the End15 scenario, we observed a 0.011 ( $p > 0.01$   $n=6$ ) increase in EI per year for a  
 350 total increase of EI by 0.07 in 2020. This increase in EI in the End10 scenario is approximately 4  
 351 times smaller than the decrease of the baseline in this same period at 0.022 per year, while in the  
 352 End15 scenario the decrease in the baseline is at the same level as the increase at a 0.011 per year  
 353 for the End15 scenario. When restricting this evaluation to wintertime, no measurable effect is  
 354 detected. Regarding spatial variability, these changes are not uniformly distributed throughout  
 355 the domain: for example, the highest rate of change can be found in the *Yamal-GydanTundra*

356 where a yearly EI increase of 0.019 was observed from 2010, while many other regions did not  
 357 show any difference at all.  
 358



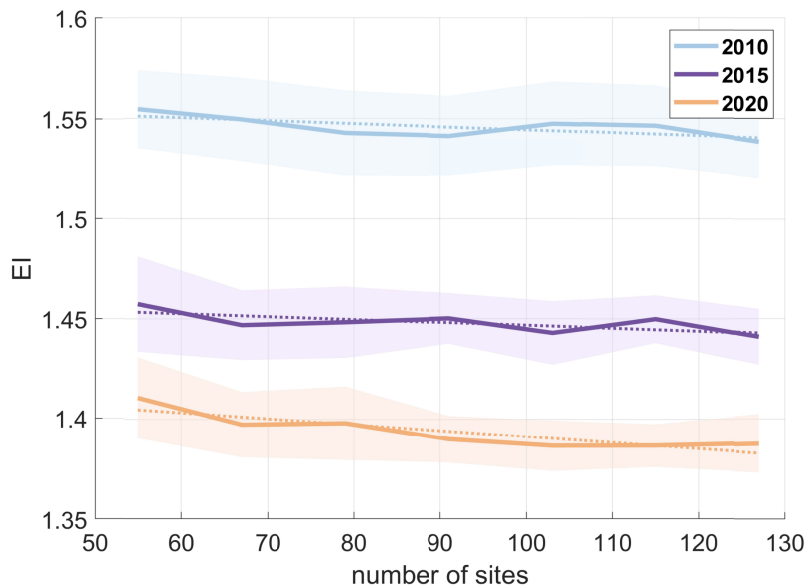
359  
 360 **Figure 3. Yearly averages in EI showing the effect of ceasing measurements from 2010**  
 361 **(End10 -purple) and 2015 (End15 - yellow) compared to the baseline (blue) which reflect**  
 362 **actual conditions. In both cases the EI became worse over time.**  
 363

364 When limiting each site's activity to 12 (Max12), 18 (Max18) and 36 months (Max36),  
 365 respectively, to investigate the effect of limited tower activity periods we found notable increases  
 366 in the EI, indicating that extended tower operation periods have a strong beneficial effect on the  
 367 reduction of upscaling uncertainties (Figure S4 d,e,f). In 2020, the average EI for Max12 was  
 368 0.38 higher than the baseline, which is equivalent to setting the network back 14 years to 2006.  
 369 For the Max18 scenario, EI was 0.27 higher than baseline, equivalent to a 12 year setback to  
 370 2008, while for Max36 a reduction in EI of 0.15 was observed, equivalent to rewinding the  
 371 network to a state 8 years ago to 2012. Across all the experiments, we find a stronger  
 372 relationship ( $R^2$  0.76,  $p > 0.001$ ,  $n=120$ ) between total mean site activity per year and negative  
 373 reciprocal transformed EI ( $-1/EI$ ) (for time passed the relation is weaker  $R^2$  0.44,  $p > 0.01$ ,  $n=120$   
 374 for total). The strong relation to the negative reciprocal of the data indicates that as more data are  
 375 added, each addition is relatively less impactful than the ones before.

376

377 The depth versus breadth analysis showed that, with the number of active months being  
 378 exactly equal, there is a slightly better network performance for multiple shorter-lived sites,  
 379 compared to fewer long active sites. In the BvD10 scenario, the maximum number of sites (127)  
 380 had a 0.016pp lower EI than the minimum number (55), while in the case of BvD15 and BvD20  
 381 these values were 0.017 and 0.024 lower, respectively. In the case of BvD10, the high and low  
 382 rating fell within each other's estimated standard deviation based on 20 replicate runs. In the  
 383 BvD15 scenario, the high value fell outside the low value's standard deviation, and in BvD20  
 384 both values fell outside each other's standard deviation (Fig. 4). Thus, as the network progresses,

385 differences between the strategies on how to distribute data months across N numbers of sites  
 386 become more pronounced.  
 387



388  
 389  
 390 **Figure 4. The impact of more shorter-lived sites (left) versus fewer longer-lived sites (right)**  
 391 **In this depth versus breadth analysis, site months equal to the combined site months of**  
 392 **2010, 2015 and 2020 (in blue, purple and yellow respectively) were pseudo randomly**  
 393 **allocated to sites to answer which performed better: more shorter-lived site or fewer longer**  
 394 **lived sites. Lines indicate the mean, dotted lines the trendline, shaded area represent one**  
 395 **standard deviation. The slopes for trendlines are  $1.5e^{-4}$ ,  $-1.5e^{-4}$  and  $-3.0e^{-4}$  for the 2010, 2015**  
 396 **and 2020 based allocations respectively. In all experiments network configurations**  
 397 **characterized by more shorter-lived sites (n=127) performed better than the few longer**  
 398 **active sites (n=55).**

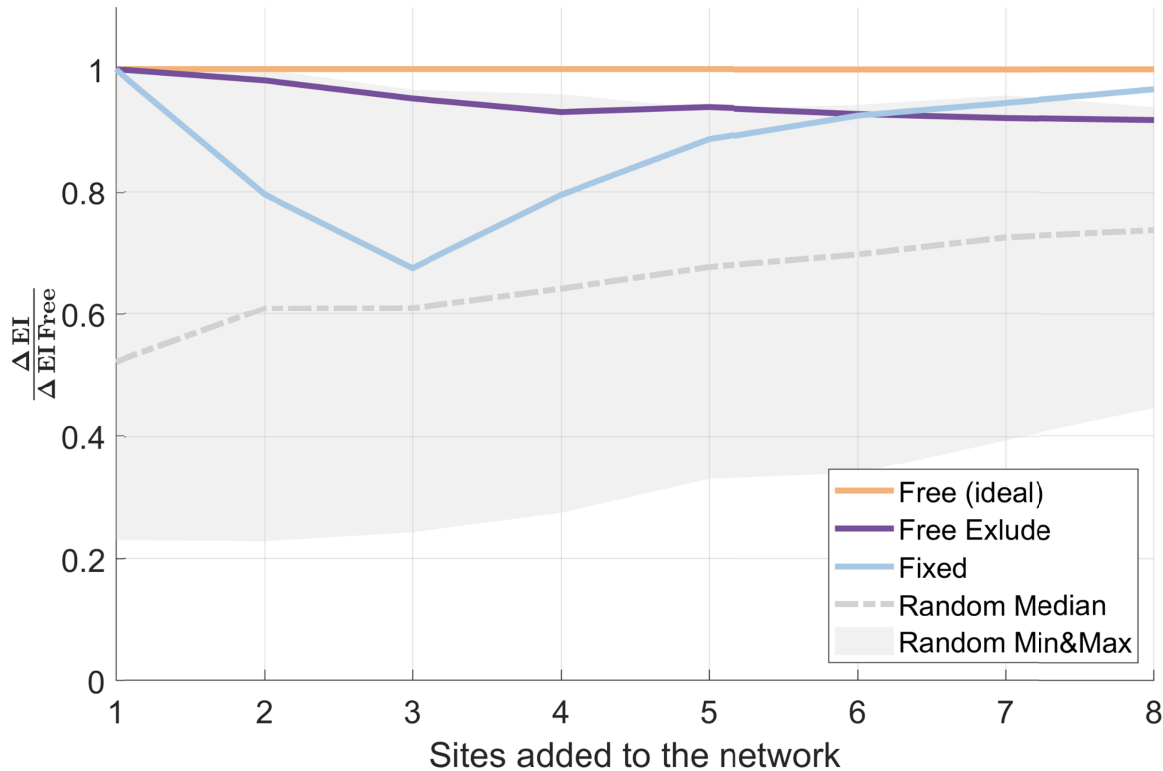
### 399 3.3 Network optimization

400 The regional network optimization conducted in the context of this study shows that in  
 401 the free optimization scenario, a single site can reduce the EI of the entire domain by as much as  
 402 0.017, while 8 sites selected from the 28 preselected sites can yield an EI reduction by up to  
 403 0.075. In the free exclude setup, where seven sites that were deemed unsuitable for network  
 404 extension were removed, the EI reduction achieved only 92% of the values obtained in the free  
 405 optimization scenario (Figure 5). Limiting the degrees of freedom of the algorithm further by  
 406 prescribing three sites resulted in an initial EI of 67% compared to the free optimization  
 407 reference, after letting the model choose the best configuration of the remaining five sites, EI  
 408 increased to 96% of the ideal optimization.

409

410 When choosing new sites randomly from the subset of 28 candidate sites, even the best  
 411 result taken from a subset of 1000 random assignments still lagged the results of the free  
 412 optimization (91%). With the median random assignment achieving an EI reduction of 74%  
 413 compared to that of the free optimization, this highlights the clear benefits of the guided

414 optimization. When less than ideal sites are initially chosen, such as tested in the free exclude  
 415 scenario, the network first drops to EI levels similar to median random assignment however,  
 416 when the optimization is allowed to choose subsequent sites it fills in the gaps and brings the EI  
 417 ratings to levels similar to the free exclude scenario, well beyond the random median (Figure 5).  
 418

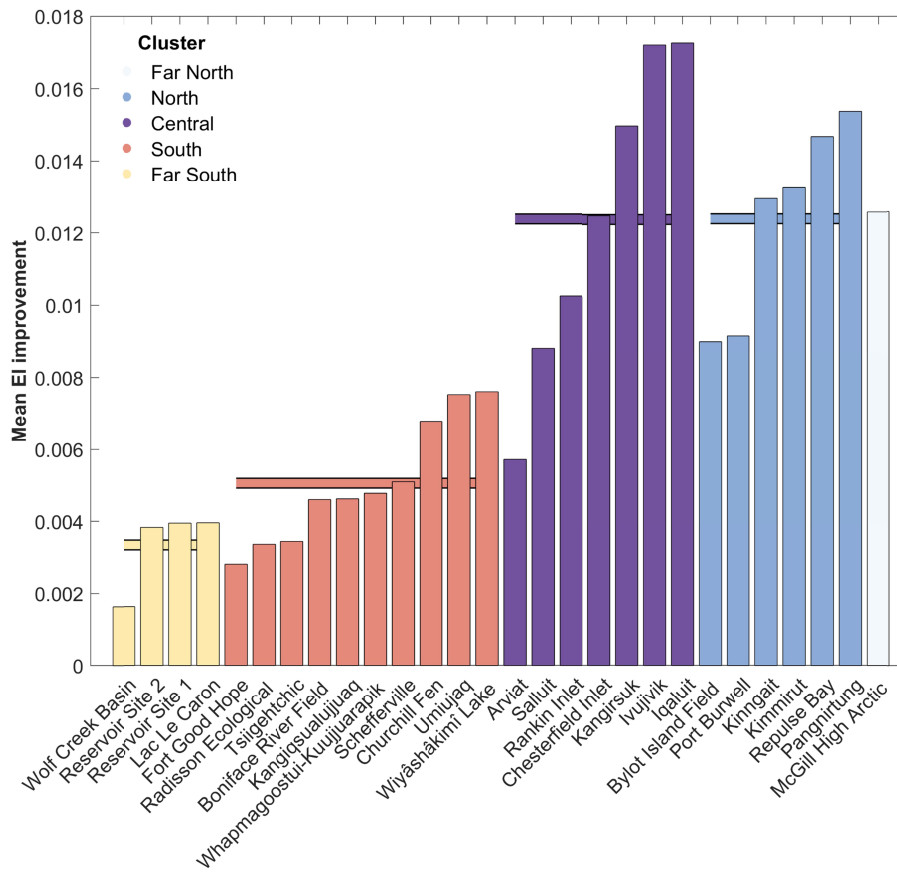


419  
 420 **Figure 5. The relative impact of network improvement scenarios**  
 421 **are shown compared to the ideal case (Free in yellow). Free exclude (purple) with seven less**  
 422 **sites for potential selections performed at 91% of the ideal case. The Fixed scenario (blue)**  
 423 **with two far less ideal sites in position two and three drops to 67% of ideal at three sites but**  
 424 **recovers after optimizing the final 5 sites to 96% of ideal. Gray lines indicate the random**  
 425 **allocation, with dashed lines indicating the mean and the dash dotted line the minimum**  
 426 **and maximum values.**

427  
 428

429 In Figure 6, the mean improvement to the network is shown for the first step of the  
 430 network optimization run. Each bar represents its site's improvement to the network if added, as  
 431 well as their clustering and mean improvement per cluster; the largest gains are present in the  
 432 three northernmost clusters. Here the optimization algorithm would select Iqaluit as the optimal  
 433 site. However, if there were practical concerns that would invalidate this location, the graph  
 434 shows that Ivugvik would be a good alternative location, both in its improvement of the network  
 435 as well as in environmental conditions, since they share a cluster. The combined use of a  
 436 similarity metric among potential sites with the EI allowed us therefore to weigh the choices of  
 437 new sites with knowledge about the location and make informed decisions when choosing  
 438 between sites without sacrificing much of the potential gains in network performance that would  
 439 come from a free optimization.  
 440

441 The Free optimization selected the following eight sites in order: Iqaluit, McGill High  
 442 Arctic Station, Ivugivik, Repulse Bay, Clearwater Lake Station, Bylot Island Field Station,  
 443 Rankin Inlet and finally Pangnirtung. This corresponds to one site from the Far North cluster,  
 444 three from the North cluster, three from the Central cluster, and one from the South cluster,  
 445 which reflects the state of the network (Figure 2) and the distribution of site improvements  
 446 shown in Figure 2 well. Sites such as McGill High Arctic and Clearwater lake are chosen before  
 447 other sites which performed better in the initial step because the addition of each site impacts the  
 448 potential benefits of other (especially similar) sites being added. Therefore for every step a new  
 449 table like Figure 5 is created, reflecting the new rankings of improvement .  
 450  
 451



452  
 453 **Figure 6. The mean improvement per site for the first network extension step in Canada**  
 454 **shown in vertical bars, clustered in 5 groups based on predictor variables to show site**  
 455 **similarity, with horizontal bars indicating the clusters mean EI improvement. Graphs like**  
 456 **these guide the expert judgment where in one view each individual site’s impact can be**  
 457 **assessed as well as their similarity to other sites. Here it is clearly shown that the greatest**  
 458 **improvement can be found in the Central, North and far North clusters.**

## 459 **4 Discussion**

### 460 4.1 Network status

461 Following the expansion of our domain (Figure 4) compared to the assessment presented  
462 by Pallandt et al. (2022), the updated representativeness maps indicate that the boreal biome in  
463 central Canada is very well represented, on par with Sweden and Finland and selected Alaskan  
464 regions. In contrast, the Arctic in Canada lacks representation by the current network of EC  
465 towers mainly at high latitudes. Considering the low number of towers in Siberia, the extension  
466 of the analysis domain further south in Russia shows that large areas are not well represented in  
467 that region. However, even in the case of relatively well represented regions, areas with poor  
468 representativeness still exist. Of note is the Aleutian island chain in Western Alaska, which is  
469 barely covered by the existing tower network. Having any type of flux measurement here thus  
470 appears to be a meaningful upgrade to the network, since, as opposed to many other  
471 underrepresented areas, these islands are neither fully mountainous nor Arctic deserts.  
472 Furthermore, this rainy region might provide important insights into how northern ecosystems  
473 might function in a future wetter climate (Bintanja & Andry, 2017). It should be noted that  
474 regions near the southern border may show elevated EI ratings, corresponding to large  
475 extrapolation errors, that may not be indicative of their actual status. The reason for this is that  
476 we do not consider sites outside the domain that could still influence it, particularly along the  
477 southern margins. The overall effect should be minimal though, since in this study we have  
478 delineated the domain based on complete ecoregions.

### 479 4.2 Extrapolation framework, and uncertainty assessment

480 The EI approach estimates how the model error increases with distance in predictor space from  
481 the training data. The distance considers different predictor importances for the defined target  
482 variable. While this yields an objectively defined and interpretable metric it is important to  
483 understand caveats of the approach. The choice of the target variable, here GPP, influences the  
484 extrapolation assessment because the target variable should determine the set of relevant  
485 predictors and associated weights used to calculate the distance to the training data. Transferring  
486 the results to other target variables would require that the set of predictors and related  
487 importances are similar to the chosen GPP target. Here we used GPP predictions from  
488 FLUXCOM extracted at site locations as target variable instead of using real EC data due to a  
489 lack of availability. This means that the estimated increase in model error with increased distance  
490 to training data in environmental space is larger than if real GPP observations were used and  
491 explains the substantially larger EI values compared to Jung et al. 2020. The model error  
492 assessed by real observations is much less sensitive to distance to training data because the error  
493 is dominated by site-specific peculiarities that are not perfectly captured, for example due to an  
494 incomplete predictor set. An incomplete predictor set further implies that we can only assess the  
495 ‘known unknowns’ by our extrapolation assessment (Jung et al. 2020). Essentially, the  
496 considerations above imply that (1) the spatial-temporal patterns of estimated EI are qualitatively  
497 meaningful but probably optimistic because the chosen predictor set and the FLUXCOM model  
498 are not perfect, and that (2) the magnitude of the estimated EI values are likely conservative, i.e.  
499 overestimated, because of using model predictions that are more sensitive to distance in predictor  
500 space compared to observations.  
501

## 502 4.3 Consideration of temporal aspects in representativeness assessments

503 Since 2011, the network representativeness assessment during winter months performs better,  
504 i.e., yields a lower averaged EI, than during summer. This finding appears counter-intuitive,  
505 since the wintertime features substantially fewer active towers, with site activity being restricted  
506 to the growing season for a large fraction of the EC towers. At the same time, spatial  
507 heterogeneity in several of the parameter grids used for upscaling, e.g. NDVIRg or NDWI, is  
508 strongly reduced and sometimes zero when snow cover is present, and due to these homogeneous  
509 conditions in the wintertime fewer towers are needed to properly reflect conditions within the  
510 upscaling domain; note though that our predictors did not include variables describing snow  
511 depth and density that might create more spatial variation in the wintertime environmental space.  
512 Accordingly, by considering temporal differences in conditions we now can show that this  
513 temporal aspect is essential to gain a full picture of the network's performance. However, to fully  
514 capture wintertime variability we should utilize actual fluxes as target since wintertime GPP is  
515 essentially zero. Finally there are increased gaps and errors in wintertime fluxes as a result of  
516 adverse measurement conditions (Oechel et al., 2014) which are not present in this dataset. Thus,  
517 while these results indicate a reduced need for wintertime monitoring, further research is  
518 required to properly account for all nuances in Arctic ecosystems.

519 From the perspective of managing a continuously operating Arctic observation network, we see a  
520 discrepancy between the funding required for proper network performance and the funding that  
521 is secured. While our historic data show that many sites stay active for longer than the prevailing  
522 three-year funding, the lack of a central, long-term funding source in many regions leads to the  
523 discontinuation of EC towers that fill crucial positions within the network. Our results highlight  
524 that network representativeness scales with the number of total active months in the dataset, and  
525 that continued, long-term measurements are required since our knowledge of the region's fluxes  
526 will eventually deteriorate in the absence of new measurements especially with increasing  
527 disturbances, ecosystem shifts, and climate change. In addition to upscaling potential of the  
528 network, there are other reasons to aim for longer time series such as understanding the  
529 ecosystems response to changing conditions, such as (Baldocchi, 2020). In other words, even  
530 though it may be sufficient to measure for about three years to constrain a basic carbon budget  
531 for a given site, at least if those measurements are done in average site conditions and not during  
532 extreme climate or disturbance years, this amount of data is not sufficient to support long-term  
533 extrapolation studies. There are programs in place which build long term networks such as the  
534 EU based ICOS (Integrated Carbon Observation System (ICOS) Research Infrastructure, 2022)  
535 network, and USA based NEON (Schimel et al., 2007). The pan-Arctic network would benefit  
536 from having such funding sources for the entire domain.

537 The depth versus breadth analysis shows that under equal activity there is a slightly better result  
538 from the representativeness evaluation for multiple shorter lasting sites over fewer long-term  
539 sites. Combined with the results of the case study and previous work, this could lead to the  
540 conclusion that raising towers in unique new locations is more impactful than long site activity in  
541 a singular space. However, there are other factors to consider beyond regional upscaling. With a  
542 focus on breadth, we might lose understanding of detailed local processes: as the ecosystem and  
543 climate changes, ecosystems respond and new processes and disturbances may happen, which  
544 could be missed or only detected after a considerably longer time. Furthermore, the cost of  
545 maintaining a tower is one to two orders of magnitude lower than establishing a new tower,

546 where the instrument cost (ICOS ERIC, 2020) and the costs for permits and construction are by  
547 far the largest investments. Since the total site months of the network is the most important  
548 indicator of EI, the most cost effective method to extend this is by keeping existing towers  
549 operational. New towers should then ideally be located in underrepresented regions as selected  
550 by this or similar methods, while still answering the project's research questions. In cases where  
551 there is no direct experimental need to remain in one location for a long time, from the  
552 perspective of the network as a whole, it would be efficient to rotate equipment between several  
553 locations. If, at the start of an experiment, power and a tower structure are erected at several  
554 locations, then the instruments can be rotated between these sites with relative ease. The results  
555 from the Endx experiments show that loss of representativeness represented by increase of EI are  
556 relatively slow, therefore gaps should be manageable when considering flux upscaling, and when  
557 one would return at regular intervals it allows for any correction of accelerated change in the  
558 ecosystem. Furthermore, many remote locations have low expected fluxes (Lafleur et al., 2012;  
559 Virkkala et al., 2021); temporary or mobile towers could be ideal to add representativeness of  
560 such locations to the network without having to make the investment of a permanent tower.  
561 Drone campaigns such as polar Modular Observation Solutions for Earth Systems camping can  
562 fulfill a similar purpose. It is clear from these analyses (Figure 3 and 6) that as far as network  
563 design is concerned to fill the gaps the EC community has to focus on less accessible locations,  
564 even though this comes at increased costs.

565 The results of the Endx experiments should be considered a conservative estimate with actual EI  
566 increase likely higher. Several of the input rasters used are static over the years. And while  
567 measurements such as NBAR will not see significant change on these time scales, data such as  
568 Enhanced Vegetation Index, Land cover and Maximum Day Time Land Surface Temperature are  
569 expected to change and not remain static. If these layers were dynamic, variations over time in  
570 these variables would increase and so would the EI when no new measurements are taken.  
571 Furthermore, the Arctic is changing at an accelerating rate (Box et al., 2019), in the absence of  
572 measurements this leads to an accelerated increase of the EI as known conditions are  
573 increasingly exceeded. All of these arguments again speak for the continuation of long-term  
574 experiments.

#### 575 4.4 Network expansion strategies

576 We have shown here that utilizing a model-guided approach to network extension greatly  
577 outperforms a random allocation (to the same feasible locations), and that this holds true even  
578 when we include less ideal choices since the model can compensate for this with further  
579 selections. As expected from the EI map in Figure 2, there is a clear preference for more northern  
580 locations. It should be noted though that this optimization was aimed at reducing the EI, the  
581 relative error as a function of distance to closest sites, which does not include the magnitude of  
582 the individual fluxes. If flux magnitude were to be considered in the metric, high-latitude sites  
583 would be comparatively less likely to be selected owing to typically lower fluxes. However such  
584 inclusion would add additional complexity and potential biases as it would either require a model  
585 ensemble to establish error magnitudes of the fluxes (Jung et al., 2020) or a weighting of the  
586 errors by expected fluxes with ambiguity on the weight the magnitude should have.

587 When choosing a location for a new site, methods like these where representativeness-based  
588 optimization models are used in tandem with expert knowledge combine the best of two worlds.

589 The modeling component grants objective insights in a potential site's impact to the network and  
590 its relation to other sites, and the expert can easily consider aspects that are too unwieldy or  
591 impossible to properly model, such as experimental design, infrastructure, and advice and  
592 requests from local communities. Quantifying tradeoffs further helps the decision-making  
593 process especially with clear visualizations.

## 594 **Conclusion**

595 We have shown that the high-latitude EC network has grown considerably over time, with  
596 significant increases in representativeness. This analysis also shows that the coverage of the EC  
597 network still needs to be improved for estimating more robust Arctic-boreal carbon budgets.  
598 Large improvements are needed especially in the highest latitudes, mountainous regions and  
599 large parts of Russia. However, improving the network requires relatively more effort with each  
600 site addition since each additional site will have comparatively less impact than the ones before  
601 as the data space is steadily filled. At the same time, we see that the largest gaps are in more  
602 remote locations, further adding to the difficulty of expansion.

603 To further guide the growth of the network we have demonstrated a network optimization  
604 method that greatly outperforms a random approach in a case study where we optimize the  
605 network by considering future expansions in the Canadian Arctic. We illustrate a way to merge  
606 representativeness based optimized network design with expert knowledge in an iterative way  
607 that incorporates understanding, local knowledge, and other hard to quantify factors.

608 Beyond extending the network it has become clear that we cannot be complacent with the  
609 existing network, as gaps in data and cessation of measurements will not only freeze our  
610 knowledge but deteriorate our ability to understand the carbon cycle. This is especially the case  
611 since rapid climate change in the Arctic is bound to move conditions further from past  
612 measurements. This is exacerbated by acceleration at which the high latitudes are changing as a  
613 result of climate change. And since total site months are central to increasing network  
614 representativeness, it is therefore of importance that existing sites should remain active and be  
615 funded for as long as possible in addition to efforts to extend the network to underrepresented  
616 locations.

## 617 **Acknowledgements**

618 None of the authors report any affiliations or financial interests that cause conflicts of interest.  
619 This work was supported by the Max Planck Society and through funding by the European  
620 Commission (INTAROS project, H2020-BG-09-2016, grant agreement no. 727890), and also by  
621 the European Research Council (ERC) under the European Union's Horizon 2020 research and  
622 innovation programme (grant agreement No 951288, Q-Arctic). Additional support for this work  
623 came from the TED Audacious Project and Woodwell Climate Research Center's Fund For  
624 Climate Solutions Project. Kyle A. Arndt is additionally supported by NSF Office of Polar  
625 Programs grant no. 2316114. The article processing charges for this open-access publication  
626 were covered by the Max Planck Society. We would like to thank Michał Gałkowski for his  
627 review of this manuscript.

628 **Open Research**

629 Table 1 lists all original MODIS data codes for raster datasets used in this research, and is  
 630 available at <https://lpdaac.usgs.gov/products>, these products have been regrided for use with  
 631 FLUXCOM those versions can be found in the Max Planck Institute for Biogeochemistry data  
 632 portal at <https://www.bgc-jena.mpg.de/geodb/projects/Home.php> file id 260. EC site metadata is  
 633 available at <https://cosima.nceas.ucsb.edu/carbon-flux-sites/>. This is an active database that is  
 634 constantly updated, for transparency a snapshot of the EC component of this database used for  
 635 this paper is retained and available on request by reviewers. EI code is from Jung et al. (2020)  
 636 with specific details in supplement 2. All analyses were performed using matlab (The  
 637 MathWorks Inc, 2022), Figures were produced in matlab, Figure 1 was produced with the  
 638 addaxis addon to plot an extra axis (Lee, 2023), and Figure 2 utilized the shaded area error bar  
 639 plot addon for the std shading (Martínez-Cagigal, 2023) , Figure 2 and S2 was created as geotiff  
 640 in matlab and then finalized using Qgis (QGIS Development Team, 2009).

641 **References**

- 642 Baldocchi, D. D. (2003). Assessing the eddy covariance technique for evaluating carbon dioxide exchange rates of  
 643 ecosystems: past, present and future. *Global Change Biology*, 9(4), 479–492.  
 644 <https://doi.org/10.1046/j.1365-2486.2003.00629.x>
- 645 Baldocchi, D. D. (2020). How eddy covariance flux measurements have contributed to our understanding of Global  
 646 Change Biology. *Global Change Biology*, 26(1), 242–260. <https://doi.org/10.1111/gcb.14807>
- 647 Banko, M., & Brill, E. (2001). Mitigating the Paucity-of-Data Problem: Exploring the Effect of Training Corpus  
 648 Size on Classifier Performance for Natural Language Processing. In *Proceedings of the First International  
 649 Conference on Human Language Technology Research*. Retrieved from <https://aclanthology.org/H01-1052>
- 650 Bintanja, R., & Andry, O. (2017). Towards a rain-dominated Arctic. *Nature Climate Change*, 7(4), 263–267.  
 651 <https://doi.org/10.1038/nclimate3240>
- 652 Birch, L., Schwalm, C. R., Natali, S., Lombardozzi, D., Keppel-Aleks, G., Watts, J., et al. (2021). Addressing biases  
 653 in Arctic–boreal carbon cycling in the Community Land Model Version 5. *Geoscientific Model  
 654 Development*, 14(6), 3361–3382. <https://doi.org/10.5194/gmd-14-3361-2021>
- 655 Bosveld, F. C., & Beljaars, A. C. M. (2001). The impact of sampling rate on eddy-covariance flux estimates.  
 656 *Agricultural and Forest Meteorology*, 109(1), 39–45. [https://doi.org/10.1016/S0168-1923\(01\)00257-X](https://doi.org/10.1016/S0168-1923(01)00257-X)
- 657 Box, J. E., Colgan, W. T., Christensen, T. R., Schmidt, N. M., Lund, M., Parmentier, F.-J. W., et al. (2019). Key  
 658 indicators of Arctic climate change: 1971–2017. *Environmental Research Letters*, 14(4), 045010.  
 659 <https://doi.org/10.1088/1748-9326/aafc1b>

- 660 Byrne, B., Baker, D. F., Basu, S., Bertolacci, M., Bowman, K. W., Carroll, D., et al. (2023). National CO<sub>2</sub> budgets  
661 (2015–2020) inferred from atmospheric CO<sub>2</sub> observations in support of the global stocktake. *Earth System  
662 Science Data*, 15(2), 963–1004. <https://doi.org/10.5194/essd-15-963-2023>
- 663 Chu, H., Luo, X., Ouyang, Z., Chan, W. S., Dengel, S., Biraud, S. C., et al. (2021). Representativeness of Eddy-  
664 Covariance flux footprints for areas surrounding AmeriFlux sites. *Agricultural and Forest Meteorology*,  
665 301–302, 108350. <https://doi.org/10.1016/j.agrformet.2021.108350>
- 666 Desai, A. R. (2010). Climatic and phenological controls on coherent regional interannual variability of carbon  
667 dioxide flux in a heterogeneous landscape. *Journal of Geophysical Research: Biogeosciences*, 115(G3),  
668 G00J02. <https://doi.org/10.1029/2010JG001423>
- 669 Göckede, M., Rebmann, C., & Foken, T. (2004). A combination of quality assessment tools for eddy covariance  
670 measurements with footprint modelling for the characterisation of complex sites. *Agricultural and Forest  
671 Meteorology*, 127(3), 175–188. <https://doi.org/10.1016/j.agrformet.2004.07.012>
- 672 Hoffman, F. M., Kumar, J., Mills, R. T., & Hargrove, W. W. (2013). Representativeness-based sampling network  
673 design for the State of Alaska. *Landscape Ecology*, 28(8), 1567–1586. [https://doi.org/10.1007/s10980-013-  
9902-0](https://doi.org/10.1007/s10980-013-<br/>674 9902-0)
- 675 Hugelius, Gustaf, Loisel, J., Chadburn, S., Jackson, R. B., Jones, M., MacDonald, G., et al. (2020). Large stocks of  
676 peatland carbon and nitrogen are vulnerable to permafrost thaw. *Proceedings of the National Academy of  
677 Sciences*, 117(34), 20438–20446. <https://doi.org/10.1073/pnas.1916387117>
- 678 ICOS ERIC. (2020). *ICOS Handbook 2020* (2nd rev. ed.). Helsinki: ICOS ERIC. Retrieved from [https://www.icos-  
cp.eu/resources/reports-and-documents](https://www.icos-<br/>679 cp.eu/resources/reports-and-documents)
- 680 Integrated Carbon Observation System (ICOS) Research Infrastructure. (2022). *ICOS Handbook 2022*. Helsinki:  
681 ICOS ERIC. Retrieved from <https://www.icos-cp.eu/resources/brochures>
- 682 IPCC. (2014). *Climate Change 2014: Synthesis Report. Contribution of Working Groups I, II and III to the Fifth  
683 Assessment Report of the Intergovernmental Panel on Climate Change* (p. 151). Geneva, Switzerland:  
684 IPCC. Retrieved from [https://www.ipcc.ch/pdf/assessment-  
report/ar5/syr/SYR\\_AR5\\_FINAL\\_full\\_wcover.pdf](https://www.ipcc.ch/pdf/assessment-<br/>685 report/ar5/syr/SYR_AR5_FINAL_full_wcover.pdf)
- 686 Ito, A., Li, T., Qin, Z., Melton, J. R., Tian, H., Kleinen, T., et al. (2023). Cold-Season Methane Fluxes Simulated by  
687 GCP-CH<sub>4</sub> Models. *Geophysical Research Letters*, 50(14), e2023GL103037.

- 688 <https://doi.org/10.1029/2023GL103037>
- 689 Jung, M., Reichstein, M., Margolis, H. A., Cescatti, A., Richardson, A. D., Arain, M. A., et al. (2011). Global  
690 patterns of land-atmosphere fluxes of carbon dioxide, latent heat, and sensible heat derived from eddy  
691 covariance, satellite, and meteorological observations. *Journal of Geophysical Research: Biogeosciences*,  
692 *116*(G3), G00J07. <https://doi.org/10.1029/2010JG001566>
- 693 Jung, M., Schwalm, C., Migliavacca, M., Walther, S., Camps-Valls, G., Koirala, S., et al. (2020). Scaling carbon  
694 fluxes from eddy covariance sites to globe: synthesis and evaluation of the FLUXCOM approach.  
695 *Biogeosciences*, *17*(5), 1343–1365. <https://doi.org/10.5194/bg-17-1343-2020>
- 696 Kljun, N., Rotach, M. W., & Schmid, H. P. (2002). A three-dimensional backward Lagrangian footprint model for a  
697 wide range of boundary-layer stratifications. *Boundary-Layer Meteorology*, *103*, 205–226.
- 698 Lafleur, P. M., Humphreys, E. R., St. Louis, V. L., Myklebust, M. C., Papakyriakou, T., Poissant, L., et al. (2012).  
699 Variation in Peak Growing Season Net Ecosystem Production Across the Canadian Arctic. *Environmental*  
700 *Science & Technology*, *46*(15), 7971–7977. <https://doi.org/10.1021/es300500m>
- 701 Lee, H. (2023). addaxis. Retrieved from <https://www.mathworks.com/matlabcentral/fileexchange/9016-addaxis>
- 702 Loescher, H. W., Law, B. E., Mahrt, L., Hollinger, D. Y., Campbell, J., & Wofsy, S. C. (2006). Uncertainties in, and  
703 interpretation of, carbon flux estimates using the eddy covariance technique. *Journal of Geophysical*  
704 *Research: Atmospheres*, *111*(D21). <https://doi.org/10.1029/2005JD006932>
- 705 Martínez-Cagigal, V. (2023). Shaded area error bar plot. Retrieved from  
706 <https://www.mathworks.com/matlabcentral/fileexchange/58262-shaded-area-error-bar-plot>
- 707 Meredith, M., Sommerkorn, M., Cassotta, S., Derksen, C., Ekaykin, A., Hollowed, A., et al. (2019). *Polar Regions*.  
708 *Chapter 3, IPCC Special Report on the Ocean and Cryosphere in a Changing Climate*. Geneva,  
709 Switzerland: IPCC. Retrieved from <https://www.ipcc.ch/srocc/>
- 710 Meyer, H., & Pebesma, E. (2021). Predicting into unknown space? Estimating the area of applicability of spatial  
711 prediction models. *Methods in Ecology and Evolution*, *12*(9), 1620–1633. [https://doi.org/10.1111/2041-](https://doi.org/10.1111/2041-210X.13650)  
712 [210X.13650](https://doi.org/10.1111/2041-210X.13650)
- 713 Natali, S. M., Watts, J. D., Rogers, B. M., Potter, S., Ludwig, S. M., Selbmann, A.-K., et al. (2019). Large loss of  
714 CO<sub>2</sub> in winter observed across the northern permafrost region. *Nature Climate Change*, *9*(11), 852–857.  
715 <https://doi.org/10.1038/s41558-019-0592-8>

- 716 Oechel, W. C., Laskowski, C. A., Burba, G., Gioli, B., & Kalhori, A. A. M. (2014). Annual patterns and budget of  
717 CO<sub>2</sub> flux in an Arctic tussock tundra ecosystem. *Journal of Geophysical Research: Biogeosciences*,  
718 *119*(3), 323–339. <https://doi.org/10.1002/2013JG002431>
- 719 Olson, D. M., Dinerstein, E., Wikramanayake, E. D., Burgess, N. D., Powell, G. V. N., Underwood, E. C., et al.  
720 (2001). Terrestrial Ecoregions of the World: A New Map of Life on Earth: A new global map of terrestrial  
721 ecoregions provides an innovative tool for conserving biodiversity. *BioScience*, *51*(11), 933–938.  
722 [https://doi.org/10.1641/0006-3568\(2001\)051\[0933:TEOTWA\]2.0.CO;2](https://doi.org/10.1641/0006-3568(2001)051[0933:TEOTWA]2.0.CO;2)
- 723 Pallandt, M. M. T. A., Kumar, J., Mauritz, M., Schuur, E. A. G., Virkkala, A.-M., Celis, G., et al. (2022).  
724 Representativeness assessment of the pan-Arctic eddy covariance site network and optimized future  
725 enhancements. *Biogeosciences*, *19*(3), 559–583. <https://doi.org/10.5194/bg-19-559-2022>
- 726 Pastorello, G., Trotta, C., Canfora, E., Chu, H., Christianson, D., Cheah, Y.-W., et al. (2020). The FLUXNET2015  
727 dataset and the ONEFlux processing pipeline for eddy covariance data. *Scientific Data*, *7*(1), 225.  
728 <https://doi.org/10.1038/s41597-020-0534-3>
- 729 Peltola, O., Vesala, T., Gao, Y., Rätty, O., Alekseychik, P., Aurela, M., et al. (2019). Monthly gridded data product  
730 of northern wetland methane emissions based on upscaling eddy covariance observations. *Earth System*  
731 *Science Data*, *11*(3), 1263–1289. <https://doi.org/10.5194/essd-11-1263-2019>
- 732 QGIS Development Team. (2009). QGIS Geographic Information System. Open Source Geospatial Foundation.  
733 Retrieved from <http://qgis.osgeo.org>
- 734 Rannik, Ü., Aubinet, M., Kurbanmuradov, O., Sabelfeld, K. K., Markkanen, T., & Vesala, T. (2000). Footprint  
735 analysis for measurements over a heterogeneous forest. *Boundary-Layer Meteorology*, *97*, 137–166.
- 736 Rantanen, M., Kämäräinen, M., Niittynen, P., Phoenix, G. K., Lenoir, J., Maclean, I., et al. (2023). Bioclimatic atlas  
737 of the terrestrial Arctic. *Scientific Data*, *10*(1), 40. <https://doi.org/10.1038/s41597-023-01959-w>
- 738 Schimel, D., Hargrove, W., Hoffman, F., & MacMahon, J. (2007). NEON: a hierarchically designed national  
739 ecological network. *Frontiers in Ecology and the Environment*, *5*(2), 59–59. [https://doi.org/10.1890/1540-9295\(2007\)5\[59:NAHDNE\]2.0.CO;2](https://doi.org/10.1890/1540-9295(2007)5[59:NAHDNE]2.0.CO;2)
- 740
- 741 Schmid, H. P. (1997). Experimental design for flux measurements: matching scales of observations and fluxes.  
742 *Agricultural and Forest Meteorology*, *87*(2), 179–200. [https://doi.org/10.1016/S0168-1923\(97\)00011-7](https://doi.org/10.1016/S0168-1923(97)00011-7)
- 743 Schuur, E. A. G., McGuire, A. D., Schädel, C., Grosse, G., Harden, J. W., Hayes, D. J., et al. (2015). Climate change

- 744 and the permafrost carbon feedback. *Nature*, 520(7546), 171–179. <https://doi.org/10.1038/nature14338>
- 745 Schuur, Edward A. G., Bockheim, J., Canadell, J. G., Euskirchen, E., Field, C. B., Goryachkin, S. V., et al. (2008).  
746 Vulnerability of Permafrost Carbon to Climate Change: Implications for the Global Carbon Cycle.  
747 *BioScience*, 58(8), 701–714. <https://doi.org/10.1641/B580807>
- 748 Serreze, M. C., & Barry, R. G. (2011). Processes and impacts of Arctic amplification: A research synthesis. *Global*  
749 *and Planetary Change*, 77(1), 85–96. <https://doi.org/10.1016/j.gloplacha.2011.03.004>
- 750 Sulkava, M., Luysaert, S., Zaehle, S., & Papale, D. (2011). Assessing and improving the representativeness of  
751 monitoring networks: The European flux tower network example. *Journal of Geophysical Research:*  
752 *Biogeosciences*, 116(G3), G00J04. <https://doi.org/10.1029/2010JG001562>
- 753 The MathWorks Inc. (2022). MATLAB (Version 9.10.0. (R2021a)). Natick, Massachusetts, United States: The  
754 MathWorks Inc. Retrieved from <https://www.mathworks.com>
- 755 Ueyama, M., Iwata, H., Harazono, Y., Euskirchen, E. S., Oechel, W. C., & Zona, D. (2013). Growing season and  
756 spatial variations of carbon fluxes of Arctic and boreal ecosystems in Alaska (USA). *Ecological*  
757 *Applications*, 23(8), 1798–1816. <https://doi.org/10.1890/11-0875.1>
- 758 Vesala, T., Kljun, N., Rannik, U., Rinne, J., Sogachev, A., Markkanen, T., et al. (2008). Flux and concentration  
759 footprint modelling: state of the art. *Environmental Pollution (Barking, Essex: 1987)*, 152(3), 653–666.  
760 <https://doi.org/10.1016/j.envpol.2007.06.070>
- 761 Villarreal, S., & Vargas, R. (2021). Representativeness of FLUXNET Sites Across Latin America. *Journal of*  
762 *Geophysical Research: Biogeosciences*, 126(3), e2020JG006090. <https://doi.org/10.1029/2020JG006090>
- 763 Virkkala, A.-M., Aalto, J., Rogers, B. M., Tagesson, T., Treat, C. C., Natali, S. M., et al. (2021). Statistical upscaling  
764 of ecosystem CO<sub>2</sub> fluxes across the terrestrial tundra and boreal domain: regional patterns and  
765 uncertainties. *Global Change Biology*, n/a(n/a). <https://doi.org/10.1111/gcb.15659>
- 766 Ward, J. H. (1963). Hierarchical Grouping to Optimize an Objective Function. *Journal of the American Statistical*  
767 *Association*, 58(301), 236–244. <https://doi.org/10.1080/01621459.1963.10500845>
- 768 Wisz, M. S., Hijmans, R. J., Li, J., Peterson, A. T., Graham, C. H., Guisan, A., & Group, N. P. S. D. W. (2008).  
769 Effects of sample size on the performance of species distribution models. *Diversity and Distributions*,  
770 14(5), 763–773. <https://doi.org/10.1111/j.1472-4642.2008.00482.x>
- 771 Xiao, J., Chen, J., Davis, K. J., & Reichstein, M. (2012). Advances in upscaling of eddy covariance measurements of

772 carbon and water fluxes. *Journal of Geophysical Research: Biogeosciences*, 117(G1), G00J01.

773 <https://doi.org/10.1029/2011JG001889>